IEEE Access
Multidisciplinary | Rapid Review | Open Access Journal

Received August 24, 2018, accepted September 29, 2018, date of publication October 16, 2018, date of current version November 14, 2018.

Digital Object Identifier 10.1109/ACCESS.2018.2875757

Ventilation Cooling Design for a Novel 350-MW Air-Cooled Turbo Generator

GUANG-HOU ZHOU[1], LI HAN[1], ZHEN-NAN FAN[2], HAI-BO ZHANG[3], XIU-CHENG DONG[2], JUN WANG[2], ZHANG SUN[2], AND BI-DE ZHANG[2]

[1]State Key Laboratory of Power Transmission Equipment & System Security and New Technology, Chongqing University, Chongqing 400030, China
[2]The Key Laboratory of Fluid and Power Machinery, Ministry of Education, Xihua University, Chengdu 610039, China
[3]Dongfang Electric Machinery Co., Ltd., Deyang 618000, China

Corresponding author: Zhen-nan Fan (fanzhennan@126.com)

This work was supported in part by the National Natural Sciences Fund Youth Fund of China under Grant 51607146 and Grant 61703345, in part by the Key Scientific Research Fund Project of Xihua University under Grant Z1520907 and Grant Z1520909, in part by the Key Research Fund Projects of Si Chuan Provincial Education Department under Grant 16ZA0155 and Grant 16ZB0159, in part by the Sichuan Science and Technology Program under Grant 2018GZ0391, Grant 2017GZ0358, and Grant 2017JY0204, in part by the Sichuan Province Key Laboratory of Power Electronics Energy-saving Technologies & Equipment under Grant szjj2016-048, in part by a grant from the Chunhui Project Foundation of the Education Department of China under Grant Z2016144, and in part by The Key Laboratory of Fluid and Power Machinery, Ministry of Education, Xihua University, Chengdu, China.

ABSTRACT Herein, we successfully designed a ventilation system for a new 350-MW air-cooled turbo-generator based on a reasonable lectotype choice and optimization analysis. Fluid field and thermal analysis based on computational fluid dynamics were performed to guide the optimization of cooling structures and ensure temperature rise under the limit of insulation grade B. The measured values obtained from recent factory assembly-type testing were found to coincide with the design expectations for generator efficiency and temperature rise. The results confirmed the feasibility of a multi-chamber forward-flow cooling path for 400-MVA-class air-cooled generators.

INDEX TERMS Air-cooled turbo generator, computational fluid dynamics, efficiency test, type test, temperature rise, ventilation cooling.

I. INTRODUCTION

Air-cooled turbo generators are suitable for gas–steam combined cycle systems owing to their advantages such as easy operation and low-cost maintenance. Over the past two decades, with the development of gas turbine technology, the demand for large air-cooled turbo generators has increased rapidly in China. To further expand its market share in power generation equipment, we have developed a new 350-MW-rated generator beyond the existing product line of air-cooled generators of Dongfang Electric Machinery Co., Ltd (DEC) [1]. This paper presents the studies of key turbo generator-cooling technologies, including scheme selection, demonstration test, design calculation, structure optimization, and prototype test.

II. VENTILATION LECTOTYPE

A. CURRENT SITUATION

After the development of air cooling technology in the 1980-1990s, the efficiency of large air-cooled turbo generators is at par with the efficiency of hydrogen-cooled turbo generators. Most units rated below 300-MVA are designed with an enclosed forward-flow cooling path in which cold air flows into the cooling ducts directly from the axial fans fitted to the rotor ends [2], [3]. A unique and more efficient cooling scheme allows the ALSTOM TOPAIR 25 series to reach a maximum unit rating of 500-MVA. This unit is equipped with auxiliary coolers downstream of the exhaust fans [4]. The Dongfang 135-MW generator, an example of an early air-cooled product line, is equipped with a forward-flow cooling path in which the stator is axially divided into five chambers with alternating centripetal and centrifugal airflows in the ducts. This ventilation scheme is optimized for three chambers in a 150-MW unit and simplified to a single centrifugal flow chamber in a 258-MVA unit. Even this simplified scheme produces good field-cooling performance [5]. This background leads us to hypothesize that the traditional cooling path could be used in a 400-MVA-class air-cooled turbo generator with further optimization. We test this hypothesis in the early prototyping stage to ensure that the proposed turbo generator design is reasonable and economic.

B. COMPARISON OF THE FEATURES OF THE COOLING PATH

Large generators are commonly equipped with an enclosed circulating ventilation system that cools components such as the windings and the iron core. A good cooling path design for an air-cooled turbo generator should have the following features:

- low ventilation loss,
- efficient airflow utilization,
- effective temperature rise control, and
- simple structures for easy manufacturing and maintenance.

Most rotor windings of large turbo generators are fabricated using hollow conductors through which cold air can pass. The sub-slots beneath the winding slots guide the cold air into the center of the rotor to achieve a smooth temperature distribution. Several schemes can be employed at the stator side for controlling the airflow direction through the fans and the iron core. A single centrifugal flow chamber path is the simplest structure. The air blown by downstream fans directly flows into the air gap and centrifugally passes through radial ducts after mixing with hot air from the rotor's cooling channels. The significant air temperature rise in the air gap prevents this design from effectively cooling the central region of the stator. Increasing the total airflow rate is not a good solution because the low airflow utilization and additional ventilation loss will reduce the generator efficiency. Since the simplest option is not optimal, the following schemes are considered for lectotype optimization:

- Multi-chamber forward flow
- Multi-chamber reverse flow
- Single-chamber reverse flow

The main advantage of the multi-chamber cooling path is that the stator central region is cooled by alternating the flow chambers along the axis, mitigating the effect of the air gap temperature rise. The air temperature difference of coolers (ΔT_{air}) could be configured as 40 K with this design, and the total demand of the airflow is considerably reduced to half the level needed for single-chamber cooling. To avoid heating the cold air by the winding ends, the top hood of the forward-flow cooling path is equipped with auxiliary coolers, as shown in Figure 1. This improves stator cooling but has no effect on the rotor side.

Reverse flow paths equipped with downstream auxiliary coolers are considerably effective from the perspective of efficiency optimization. The elimination of fan preheating further decreases the reference temperatures of both stator and rotor by 10 K and increases ΔT_{air} up to 50 K. This change reduces the airflow demand and ventilation loss. However, the structure of a multi-chamber reverse-flow cooling path (Figure 2) is too complicated for use in a 350-MW turbo generator. Three main factors rule out this design for the present purposes. First, the generator end cover must be divided into at least outer, middle, inner chambers and the rotor shaft must be equipped with rotating draft tubes as the intake fans are upstream of the rotor-cooling channels. The optimization

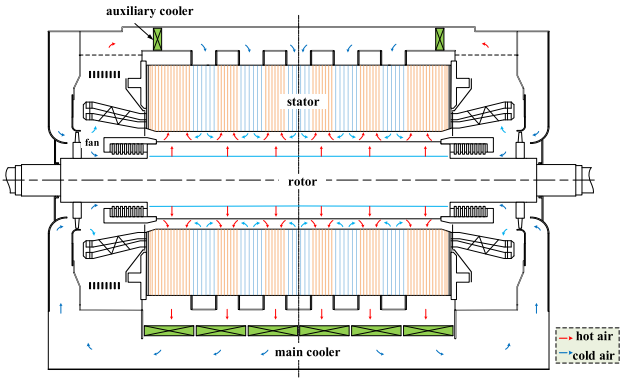

FIGURE 1. Multi-chamber forward-flow cooling path.

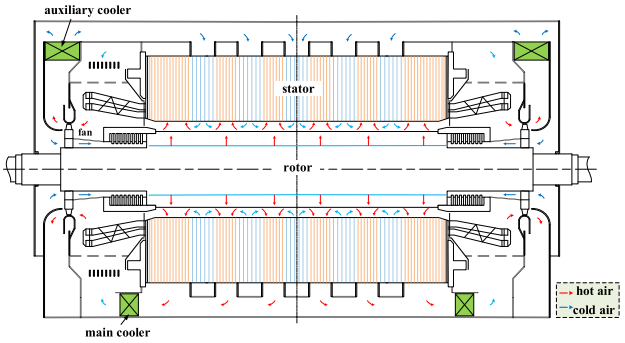

FIGURE 2. Multi-chamber reverse-flow cooling path.

of the aerodynamic characteristics of these parts would be time-consuming and expensive. Second, the main coolers and perforated annular cover must be installed upstream of the inner chamber to maintain moderate temperatures at the stator end winding and lead wire. Third, the dense alternating cooling chambers in the iron core needed for high airflow utilization make the assembly and sealing considerably difficult.

The assembly required for a single-chamber reverse flow path (Figure 3) is relatively simple, and this technology still allows ΔT_{air} of 50 K. The key of this design [6] is balancing the relation between reducing generator windage losses and uniform airflow in the cooling ducts. Additional perforated distribution plates along the axis on the upstream side of core ventilation ducts are necessary to achieve a uniform airflow distribution in the ducts. In this design, the air gap windage loss should be higher than that of a multi-chamber cooling path because all air from cooling channels flows into the air gap at high velocity.

C. SINGLE-CHAMBER REVERSE-FLOW VENTILATION MODEL TEST

A 0.45-scale ventilation model was designed to study the actual flow characteristics (Figure 4). At a stable speed of 3000 rpm, the air velocity and pressure were measured using type L pitot tubes and the model ventilation loss was calculated from drag motor torque measurements. The test

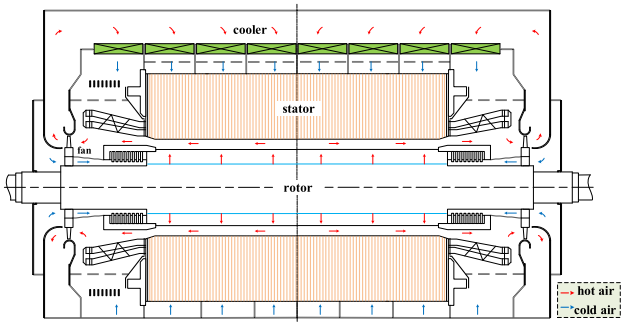

FIGURE 3. Single-chamber reverse-flow cooling path.

FIGURE 4. Single-chamber reverse-flow ventilation model.

results revealed that without perforated distribution plates, most of the cooling air flowed near the duct walls; thus, the air velocity in the center of the ducts was considerably low. With perforated distribution plates installed, the airflow distribution was acceptable for cooling; however, both the static pressure and drag power increased dramatically.

Figure 5 shows a comparison of the flow field measurements performed before and after regulating the perforated plates. The prototype characteristics were evaluated based on the following hydrodynamic similarity laws:

$$V_G/V_M = (L_G/L_M) \cdot (n_G/n_M) \quad (1)$$

$$H_G/H_M = (L_G/L_M)^2 \cdot (n_G/n_M)^2 \quad (2)$$

$$Q_G/Q_M = (L_G/L_M)^3 \cdot (n_G/n_M) \quad (3)$$

$$P_G/P_M = (L_G/L_M)^5 \cdot (n_G/n_M)^3 \quad (4)$$

The windage loss of the generator ventilation system was more than 1.6 times than that of the usual loss, thereby requiring increased exhaust fan performance. Additionally, the generator ventilation loss was more than 3300 kW and accounted for almost 65% of the total loss. This loss is not acceptable for a practical design.

Based on the above results, we preferred using the multi-chamber forward-flow cooling path for the 350-MW air-cooled generator. A thermal network analysis determined an overall cooling arrangement of 13 alternating flow chambers with six cold zones and seven hot zones.

III. DESIGN CALCULATIONS

A. PHYSICAL MODELS

Flow field and thermal analyses were performed using the CFD software package. Three-dimensional models of the

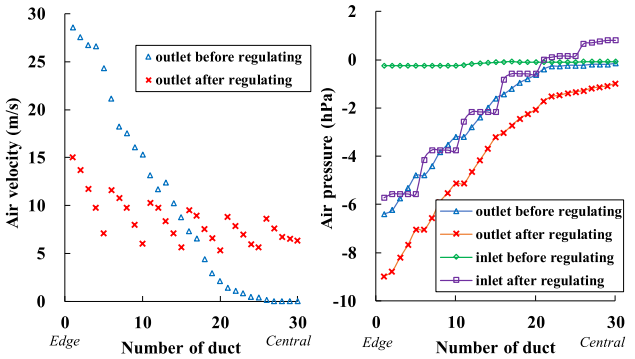

FIGURE 5. Comparison of model flow field measurements before and after regulating the perforated plates.

generator structures and the fluid domain were established individually and stitched together via couple-interfacing. The calculation domain was discretized by polyhedral meshing.

The flow field model comprised domains for the frame, air coolers, end winding, iron core, rotor surface and axial fans, as shown in Figure 6.

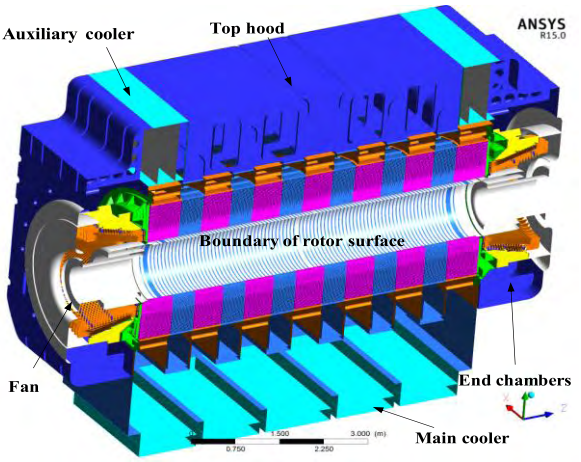

FIGURE 6. Numerical model of the airflow field (cutaway view).

The multi-reference frame (MRF) model was used to simulate the coupling relation between the stator and rotor. The mass flow inlet boundaries were set at the upstream side of axial fans, and the pressure outlet boundary was set at the downstream side of the main coolers. To account for a considerable amount of relevant structure details, the calculation domain included more than 200 million grid nodes and more than 36 million polyhedral elements.

B. MATHEMATICAL METHODS

To calculate the density, velocity, temperature, energy and turbulence in the domain, conservation equations for mass, momentum, and energy were established and numerically discretized. For any variable, the differential form of the conservation equation can be expressed as follows:

$$\frac{\partial}{\partial t}(\rho\phi) + \nabla \cdot \left(\vec{V}\rho\phi\right) = \nabla \cdot (\Gamma \nabla\phi) + S \quad (5)$$

The *RNG* k–ε two-equation turbulence model [7] was adopted to simulate the flow field. The velocity and pressure coupling equations were calculated using the SIMPLEC algorithm. The conjugate heat transfer model was adopted to simulate solid-surface convection in the interface domain. The Nusselt numbers of the cells in the first layer near a wall [8] were calculated as follows:

$$Nu = \frac{-(\partial T/\partial n)_w}{(T_w - T_m)/l} \tag{6}$$

C. RESULTS AND ANALYSIS

1) FLOW FIELD FEATURES OF RADIAL SECTION

Air flows through the top hood into the 13 iron core chambers and interfaces with the air gap. It then flows out through the bottom hood. This feature may cause nonuniform airflow distribution along the circumferential direction in stator ducts. Adjusting the throat distance $L_{\min}$ between a frame, and the core can reduce the windage loss into an appropriate range, thereby reducing the circumferential difference. Figure 7 shows the calculated flow field distribution after adjusting the throat distance. The section shown is in the centrifugal flow chamber of iron core. Although the air pressure in the upper region was higher than that in the bottom by ∼400 Pa, the circumferential distribution of the airflow in the duct was uniform.

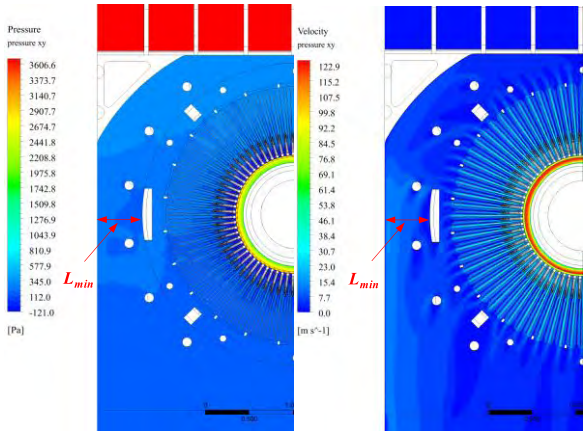

FIGURE 7. Flow field distribution of the ventilation duct section.

2) FLOW FIELD FEATURES OF THE MERIDIONAL SECTION

Figure 8 and 9 show the calculated flow streamlines and air pressure map in a generator meridional section. The segmented baffles in the top hood result in an orderly flow distribution. The air pressure drop of the auxiliary coolers was slightly higher than that of the main coolers, but together, they accounted for only a small proportion of the total air pressure drop. Most windage loss was concentrated in the ventilation ducts, and the local loss from the iron core inner surface accounted for more than half of the total loss. In the actual manufacturing process, measures, including removing the windward side of the wedge at the ventilation ducts and bending and adjusting the channel spacing at the teeth, can be taken to reduce this local loss. The result that the

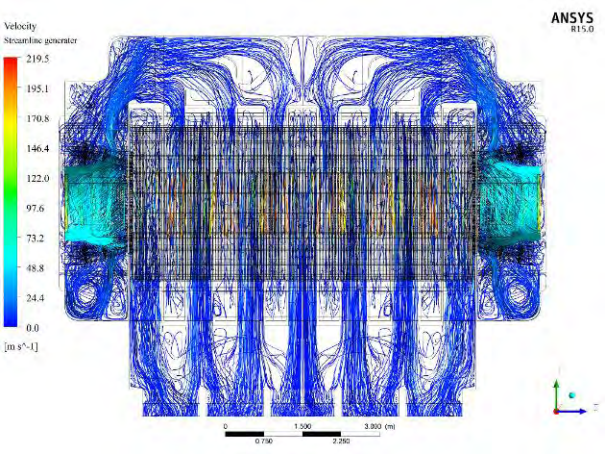

FIGURE 8. Calculated flow streamline distribution of the generator meridional section.

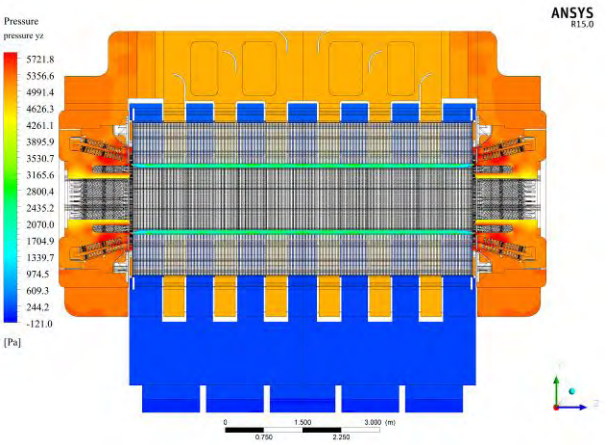

FIGURE 9. Calculated static pressure distribution of the generator meridional section.

actual measured value was reduced by 30% fully confirms the importance of such optimization measures.

The calculated airflow distributions along the rotation axis are shown in Figure 10. The airflow in the first chamber was certainly lower than that in other sections. Considering the mixing of hot air discharged from the rotor-end winding slits, the local cooling condition could be worse. Thus, some optimizations were made to the model, including adjusting the baffle clearance of air gap ends, reducing the slit section area between the press fingers, and decreasing the pitch of the ducts in the edge region. In addition, to complement the cold air supplied to the first chamber, the exhaust position of the ventilation slots at the polar end was moved nearer to the marginal ducts around the edges. The recalculated results revealed that these optimizations increased the airflow rate in the first chamber by 20%.

3) VENTILATION LOSS ANALYSIS

The aerodynamic consumption of the generator's rotating parts can be expressed as follows:

$$P_{Vent} = \sum M_t \omega_{rot} + \left(\sum q_m h_{out} - \sum q_m h_{in}\right) \tag{7}$$

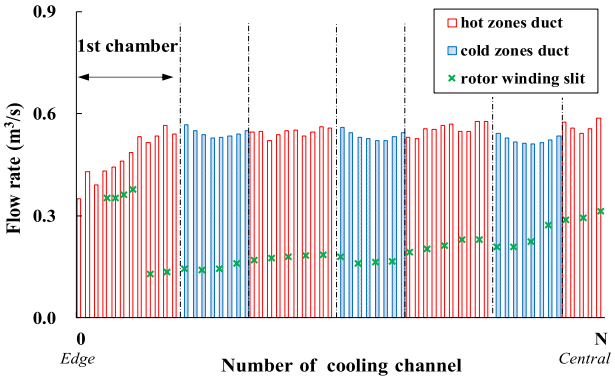

FIGURE 10. Calculated flow rate distributions of the stator ventilation ducts and rotor winding slits.

FIGURE 11. Fan aerodynamic performance of the test platform.

where M_t is the momentum acting on air from a discrete element of the rotational surface, ω_{rot} is the rotational angular speed, q_m is the mass flow rate through a discrete element of the fan inlet or outlet section, h_{in}/h_{out} is the enthalpy at a discrete element of the fan inlet or outlet section.

The first term represents the aerodynamic consumption of the rotor surface, whereas the second term represents the ventilation consumption of fans.

The aerodynamic consumption of an enclosed ventilation system was eventually translated into heat; hence, Eq. (7) can be expressed as follows:

$$P_{Vent} = c_m q_m \Delta T \tag{8}$$

where c_m is the unit mass heat capacity and ΔT is the difference in air temperature between the inlet and outlet sections of the calculation domain.

The above equations yield two different numerical solutions for generator ventilation loss. The ventilation loss was 2060 kW, accounting for nearly 40% of the generator's total loss, which is suitable for an air-cooled unit. The air temperature rise of the fans was 11.5 K. The fan static efficiency at the design point was 0.54, and aerodynamic consumption accounted for 55% of the ventilation loss. The system therefore provides the generator with a sufficient airflow rate of 88 m^3/s.

The fan aerodynamic design is based on CFD modeling as well as on full-flow performance testing. Figure 11 shows a photograph of the axial fan aerodynamic testing platform.

4) TEMPERATURE RISE CALCULATIONS AND ANALYSIS

As mentioned above, the technical difficulties associated with the multi-chamber forward-flow cooling path were focused on the rotor side. Compared with 220-MW air-cooled generators, the rotor winding loss per unit length was increased by 30% in the 350-MW generator, but the rotor diameter increased by only 4%. This indicated that assuming the same rotor-cooling design, the rotor temperature rise was at least 20% greater than that of a 220-MW generator. A study of the rotor convective heat transfer coefficients will be useful for investigating the ways in which the cooling conditions can be improved. According to the flow field analysis, a non-fully developed turbulence heat transfer model was judged to be appropriate for characterizing regions with Reynolds number above 10000, including the airgap, sub-slots, and rotor-end winding slits. The average Nusselt number of this region was calculated with a semi-empirical Eq. (9) expressed as follows:

$$Nu_t = 0.023 Re^{0.8} Pr^{0.4} C_t \tag{9}$$

where

$$C_t = \left[1 + \left(d/l\right)^{0.7}\right] \left(T_f/T_w\right)^{0.5} \tag{10}$$

The regions with Reynolds number in the range 2300-10000, particularly the radial slits of rotor winding, were characterized with the transitional flow tube heat transfer model, and the average Nusselt number was calculated using Eq. (11), which is expressed as follows:

$$Nu_s = 0.0214 \left(Re^{0.8} - 100\right) Pr^{0.4} C_s \tag{11}$$

where

$$C_s = \left[1 + \left(d/l\right)^{\frac{2}{3}}\right] \left(T_f/T_w\right)^{0.45} \tag{12}$$

A reasonable ratio of d/l can yield better convective intensity. After adjusting the structure size, the average convective heat transfer coefficients of different regions are listed as follows:

- The value of the airgap surface was 209.7 $W/m^2/K$
- The value of the sub-slots was 155.0 $W/m^2/K$
- The value of the rotor-end winding slits was 164.7 $W/m^2/K$
- The value of the radial slits was 140.6 $W/m^2/K$

According to thermal network analysis results from the rotor, the heat flow rate at the airgap surface accounted for only 14.5% of the loss, with the remaining loss occurring in the inner cooling structures. Therefore, the following measures were implemented to optimize the inner cooling structure:

- Increasing the depth of winding slots and sub-slots to improve the rotor centrifugal pressure head
- Improving the inlet structure of sub-slots to reduce the local windage loss
- Adjusting the width and transverse pitch of the winding slits to increase convective intensity

- Designing rotor wedges with irregular openings to smooth the airflow distribution at the radial slits
- Adjusting the length of branch slits and the windward air inlet to smooth the temperature rise distribution across the rotor-end winding.

The winding conjugate heat transfer calculation model comprises domains such as winding, insulation, wedge and the air region around these structures. The rotor airflow boundary is defined by the MRF method at 3000 rpm. The winding heat source is defined as the local temperature's function to improve the precision of the analytical model, which is expressed as Eq. (13):

$$q = I^2 \times \frac{(235 + t)}{(235 + 15)} R_f, \tag{13}$$

where:

t is the calculated temperature of local elements; and

R_f is the winding reference resistance under 15.

In the process, the local hot spot temperature is found to rise and is still too high for both the #7 and #8 windings. To solve this problem, the surface-cooling sub-circuit is provided by a combination of insulation support blocks between adjacent windings. The recalculated temperature field distribution of the #8 winding is shown in Figure 12.

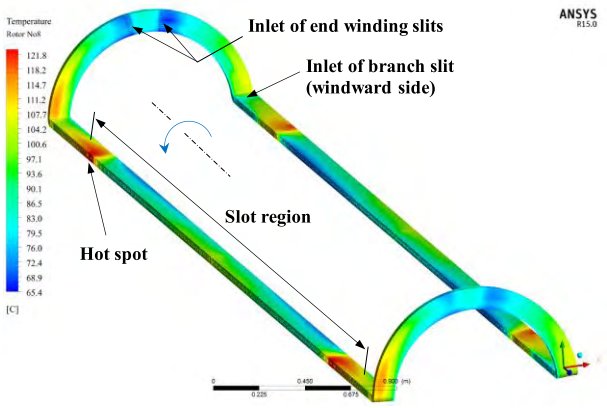

FIGURE 12. Temperature field distribution of the eighth rotor winding.

The results indicated that under the reference condition of the generator cold air temperature at 40°C, the average rotor winding temperature rise was 66.6 K, which is under the limit for insulation grade B. The local hot spot temperature rise of the conductor was 81.8 K, which is lower than the temperature rise limit for insulation grade F.

The stator temperature field was calculated using the same method, and the cooling conditions were determined via flow field analysis. Under the same reference conditions, the highest temperature rise of the stator strands was 76.1 K, which is below the limit for insulation grade F. The slot hot spot was located at the center of the first chamber. The temperature rise at the upper strands was higher than that at the lower strands by ~4-7 K on the same section. The layer insulation (position of coil RTD) temperature rise was lower than the average rise of the strands by ~10 K, and the hottest value was 63.5 K. The nose temperature was higher the temperature in the other regions of the end winding but still did not exceed the limit for insulation grade F (Figure 13).

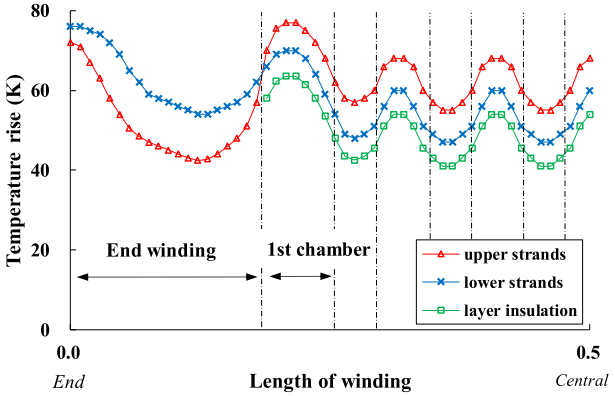

FIGURE 13. Calculated values of the stator winding temperature rise (strands and layer insulation).

According to the temperature field analysis, the CFD results were completely in conformity with the design requirements of installing an insulation material of grade F and an insulation grade B rating. These results illustrated the feasibility of using a multi-chamber forward-flow cooling path in a 400-MVA-class air-cooled generator.

IV. TEST RESEARCH

The first prototype unit for the final generator design passed factory assembly-type testing in June 2016. In the meantime, the rated temperature rise and efficiency were determined.

A. TEMPERATURE RISE AND EFFICIENCY DETERMINATION

It is considerably difficult to directly assess the rated temperature rise and efficiency under full-load conditions in a factory. Thus, a no-load short-circuit technique [9] was adopted. We obtained the measurements for four test conditions, including mechanical loss determination (idling), $1.0U_N$ no load, $1.15U_N$ no load, and $1.0I_N$ short-circuit. The rated temperature rise of the stator winding and iron core was calculated as follows:

$$\Delta T_N = \Delta T_c + \Delta T_i - \Delta T_o \tag{14}$$

where ΔT_c, ΔT_t and ΔT_0 are the measurements under the test conditions of three-phase symmetrical short-circuit, no load, and mechanical loss determination, respectively. The reference cold air temperature was corrected to 40°C for these measurements.

The rotor winding temperature rise was proportional to the winding loss; thus, the rated value was calculated using the equation shown in Figure 15.

The full-load efficiency of the generator was obtained by measuring the segregated losses. The generator ventilation loss, the airflow rate through the coolers, and the air temperature rise of the fans were measured under the test condition of

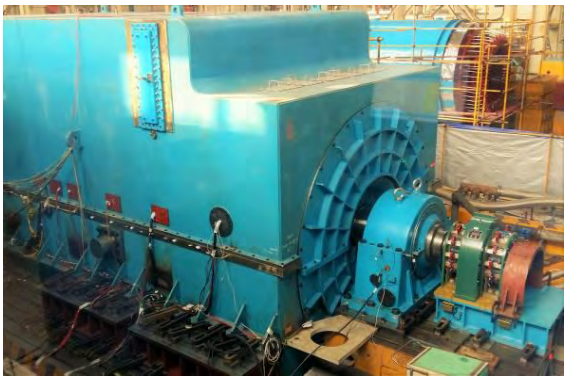

FIGURE 14. Generator assembly test site.

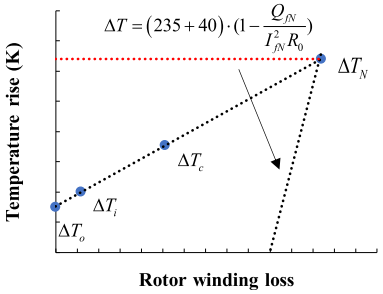

FIGURE 15. Measurement of rotor-rated temperature rise.

mechanical loss determination. Table 1 lists the measured and calculated values of the rated temperature rise and efficiency for the sake of comparison.

B. TEMPERATURE RISE DETERMINATION WITH AUXILIARY COOLERS TURNED OFF

All temperature rise data in Table 1 have margins at the limit, so the temperature rise determination with auxiliary coolers turned off was performed during factory-type testing. These measurements illustrated that the rotor average temperature rise was 68 K, which is still consistent with the expectations.

TABLE 1. Measurement and calculation data full load: active 350-MW, voltage 20 kV and power factor 0.85.

Parameters		Measured	Calculated	Guaranteed
Efficiency and full load	%	98.75	98.72	98.72
Ventilation loss	kW	1898	2060	\
Temperature rise		Measured	Calculated	Guaranteed
RTD of winding slots	K	64.0	63.5	≤80
Surface of end winding	K	69.0	67.0	≤80
Rotor winding and average	K	64.5	66.6	≤75
Air through fans	K	11.4	11.5	\
Airflow rate		Measured	Calculated	Guaranteed
Main coolers	m^3/s	96	88	\
Auxiliary coolers	m^3/s	58	56	\

The stator temperature distribution was found to coincide with the calculation results (Figure 16). The maximum winding nose temperature did not depend on the auxiliary coolers.

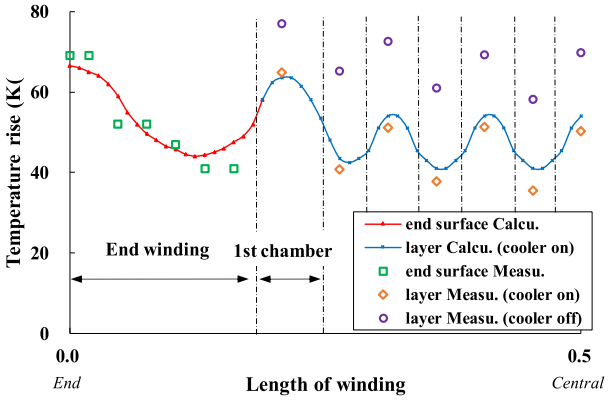

FIGURE 16. Stator-rated temperature rise with and without auxiliary coolers engaged.

When the auxiliary coolers were inactive, the winding slot temperature rise increased by 15–20 K, but the growth rate in the first chamber was lower than that in the other chambers because the cooling air from the rotor side and the axial airgap inlet was not affected by the auxiliary coolers. The maximum temperature rise of the winding slots was 77 K, still located in the center of the first chamber. These test results illustrate that with auxiliary coolers in the inactive state, the full-load temperature rise increased, which still met the design specification for long-term operation.

C. ROTOR FULL-CURRENT TEMPERATURE RISE DISTRIBUTION

During the three-phase steady-state short-circuit test, the $1.0I_{fN}$ rotor temperature rise distribution was determined with the partial winding reverse connection method [10]. Since the rotor loss and cooling conditions matched those for the full-load operation, measurements performed with this method accurately represented the actual rotor temperature rise.

It is well known that due to the complexity of the structure, materials, and ventilation of the huge air-cooled turbo generator, the temperature distribution at different locations on the rotor windings of the huge air-cooled turbo generator is complex and nonuniform. Therefore, only direct temperature measurement at several different positions on the rotor winding can truly verify the ventilation and cooling design model and results. To date, most researchers and factories have failed to conduct direct temperature measurement of turbo generator rotor windings. In previous researches, the average temperature of the rotor windings has been usually measured using the electric resistance method, which is used to indirectly verify the ventilation and cooling analysis and design results. Such verification work can neither obtain the temperature distribution trends of the rotor winding nor accurately locate the position of the highest temperature of the rotor winding; moreover, its accuracy and rationality are questionable. The main reason for the above facts is that direct measurement of the rotor winding temperature in turbo generators presents significant difficulties: first, the rotor speed of the turbo generator is so high (3000 r/min) that installing tem-

perature sensors on the rotor winding is difficult; second, owing to the strong time-varying magnetic field interference in the air gap of the generator, accurate transmission of the measurement signal is also difficult; third, the axial thermal expansion of the generator rotor winding may cause damage to the temperature-measuring sensors and the insulating material; fourth, if the temperature measurement sensors are directly mounted on the rotor windings, supplying power to them is also very difficult; finally, the test takes a long time and the cost is relatively high.

To overcome the above difficulties, we designed a new temperature measurement system to test rotor winding temperature directly, as depicted by the principle block diagram of this system in Fig. 17(a), with the details of the system shown in Figs. 17(b) and (c).

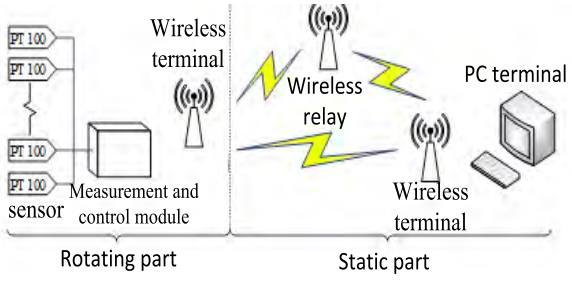

(a)

(b)

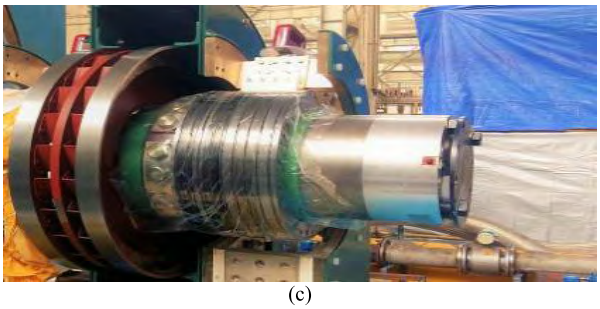

(c)

FIGURE 17. Rotor winding temperature direct measurement device. (a) Principle diagram of rotor winding temperature direct measurement system. (b) Installation position of temperature sensors. (c) Frontend module on the shaft end for wireless measurement.

In this measurement, 10 PT100 sensors were arranged on the surface of the hottest top conductor of the eighth winding and led into the rotational acquisition module on the shaft end. During testing, the frontend module transmitted the measured signal to a host computer over the 2.4-GHz band.

The measured values of the eighth rotor winding temperature rise under full-load operation conditions are shown in Figure 18. The maximum temperature rise was 84 K, which was below the limit for insulation grade F and observed in the region near the air outlet of the end winding slits. This measurement of full-current temperature rise was consistent with the calculation results, and the analysis and design results presented in this paper have been satisfactorily verified.

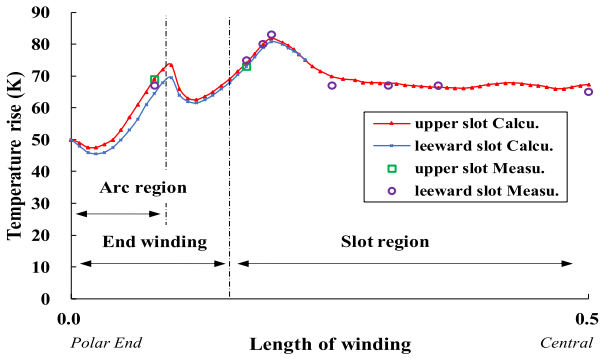

FIGURE 18. Comparison of the measured and calculated values of eighth rotor winding temperature rise during a full-load operation.

V. CONCLUSIONS

We used model tests and CFD calculations to guide the development of the ventilation cooling scheme for a new 350-MW air-cooled turbo generator. Factory-type testing of the first prototype unit showed that all measurements of the generator efficiency and temperature rise under full-load operation conditions were in good agreement with the calculation results and that none exceeded the design values. The generator can be used for a long-term full-load operation without the auxiliary coolers. This research illustrated that a multi-chamber forward-flow cooling path is suitable for such a large air-cooled generator. In addition, the cooling path is straightforward and economical. Further optimizations could improve the generator efficiency by reducing the ventilation loss and hot spot temperatures. These potential measures include design changes that make the axial fans and end winding cooling structure considerably efficient.

There are several important aspects of our proposed methodology that are worth mentioning. Although some studies and factories have already conducted research on ventilation and cooling of turbo generators, this study has the following advantages as compared with them:

First, the air-cooled turbo generator analyzed herein has a huge capacity of 350-MW, which is not only the largest air-cooled turbo generator in China, but also one of the largest air-cooled turbo generators in the world. In the design of ventilation and cooling, these large versions present unique difficulties and challenges. Simultaneously, it is worth noting that, to date, the analysis and design of ventilation and cooling of such giant air-cooled turbo generators is uncommon in previously published reports.

Second, compared with the previous studies conducted by researchers and manufacturers, the analysis and design results

presented herein have been more fully, thoroughly, and reliably verified, which provides a higher accuracy, rationality, and applicability. Therefore, our analytical model and design results are more accurate, reasonable, and applicable than most previous research.

Third, our design results have been applied in the design and manufacture of actual giant air-cooled turbo generators. As of June 30, 2018, a world famous large-scale generator design and manufacturing company, China Dongfang Electric Co., Ltd. has applied our ventilation and cooling scheme described in this paper to four 350-MW giant air-cooled turbo generators, and 22 300-MVar air-cooled condensers.

Accordingly, compared to previous research, it is our opinion that the ventilation and cooling design proposed in this paper is more effective, reliable, and advanced.

REFERENCES

[1] C. Zhao, "Development of DongFang air cooled turbo generator," *Dongfang Electr. Rev.*, vol. 16, no. 2, pp. 89–97, 2002.
[2] S. Muramatsu, K. Hattori, K. Takahashi, A. Nakahara, and K. Iwashige, "Development of 250-MVA air-cooled turbine generator," *Hitachi Rev.*, vol. 54, no. 3, pp. 121–125, 2012.
[3] C. E. Stephan, "New air-cooled turbo generator in the 300-MVA class," *Fuel Energy Abstr.*, vol. 37, no. 4, p. 273, 1996.
[4] R. Joho and B. Zimmerli, "Large air-cooled turbogenerators: Design features and operating experience," in *Proc. IEEE Int. Electr. Mach. Drives Conf.*, May 1999, pp. 755–757.
[5] H. Ling *et al.*, "Large capacity air-cooled turbine generator developed by DEC," *Large Electr. Mach. Hydraulic Turbine*, vol. 36, no. 6, pp. 13–16, 2008.
[6] D.-Y. Wu and A.-I. Wang, "Analysis and application of the flow field in ventilation ducts of intake air turb-type generator," *J. Exp. Fluid Mech.*, vol. 24, no. 5, pp. 17–21, 2010.
[7] Y. P. Lu, Q. H. Pan, X. M. Sun, and J. D. Han, "Effect of turbulence models on temperature and flow field for turbo-generator rotor," *Electr. Mach. Control*, vol. 18, no. 11, pp. 72–77, 2014.
[8] W.-Q. Tao, *Numerical Heat Transfer*. Xi'an, China: Jiao Tong Univ. Press, 2001.
[9] *IEEE Guide: Test Procedures for Synchronous Machines Part I—Acceptance and Performance Testing Part II-Test Procedures and Parameter Determination for Dynamic Analysis*, IEEE Standard 115-1995, 2002.
[10] C. Zhao, "Turbo generator rotor full-current test with method of partial winding reverse connection," *Dongfang Electr. Rev.*, vol. 3, no. 4, pp. 1–5, 1989.

GUANG-HOU ZHOU received the M.Sc. degree in electrical machine from Chongqing University, Chongqing, China, in 2007, where he is currently pursuing the Ph.D. degree with the Department of Electrical Engineering. His research interests include the field calculation, the design and control of electric machines.

LI HAN received the M.Sc. and Ph.D. degrees in electrical machine from Chongqing University, Chongqing, China, in 1986 and 2008, respectively. He is currently a Professor at Chongqing University. His research interests include the field calculation, the design and control of electric machines.

ZHEN-NAN FAN was born in Longchang, China, in 1981. He received the Ph.D. degree in electrical engineering from Chongqing University, Chongqing, China, in 2013. He is currently an Associate Professor at Xihua University. His research interests include magnetic and thermal field calculation of generators, electrical machinery, and motor drives.

HAI-BO ZHANG received the B.Eng. degree in electrical machinery from the University of Science and Technology of China, Hefei, China, in 2008. He is currently an Engineer with Dongfang Electric Machinery Co., Ltd., China. His research interests include the magnetic and thermal field calculation of generators.

XIU-CHENG DONG was born in Xianyang, China, in 1963. He is currently a Professor at Xihua University. His research interests include the control and analysis of generators, electrical machinery, and motor drives.

JUN WANG was born in Mianyang, China, in 1966. She received the Ph.D. degree in electrical engineering from Southwest Jiaotong University, Chengdu, China, in 2006. She is currently a Professor at Xihua University. Her research interests include magnetic and thermal field calculation of generators, electrical machinery, and motor drives.

ZHANG SUN was born in Lichuan, China, in 1986. He received the M.Sc. degree from Xihua University, Chengdu, China, in 2013. He is currently a Lecturer at Xihua University. His research interests include magnetic and thermal field calculation of generators, electrical machinery, and motor drives.

BI-DE ZHANG was born in 1975. He received the Ph.D. degree from Chong University in 2002. He is currently a Professor in electrical engineering with Xihua University. His research interests include on-line monitoring and fault diagnosis of electrical equipment.